Support Information

Three-Dimensional Porphyrinic Covalent Organic Frameworks for Highly Efficient Electroreduction of Carbon Dioxide

Shao-Yi Chi, Qian Chen, Shao-Shuai Zhao, Duan-Hui Si,* Qiu-Jin Wu, Yuan-Biao Huang* and Rong Cao

Section S1. Materials and Methods

All regents and chemicals were purchased without further purification. P-nitrobenzaldehyde (98%) and $SnCl{\cdot}2H_2O$ (98%) were purchased from Aladdin, $Co(OAc)_2{\cdot}4H_2O$ (98%) was purchased from Alfa. Tetra(4-formylphenyl)methane (TFPM) were purchased from EXTENSION, pyrrole (99%) was purchased from Adamas. Pyridine (C5H5N, ≥ 99.5%), Chlorobenzene, o-dichlorobenzene, DMF, *n*-butyl, acetic anhydride, acetic acid, propionic acid, acetone, concentrated ammonia, tetrahydrofuran, chloroform, concentrated hydrochloric acid, diethyl ether, NaOAc, $NaHCO_3$, and K_2CO_3 were purchased from Sinopharm Chemical Reagent Co., Ltd. All aqueous solutions were prepared with Ultrapure water (18.25 MΩ·cm).

Nuclear magnetic resonance (NMR) spectroscopy was measured at Bruker-Biospin AVANCE III spectrometer, operating at 400 MHz for ^1H NMR and 100 MHz for ^{13}C NMR. The Fourier transform infrared spectroscopy (FT-IR) were recorded using KBr pellets on a PerkinElmer Spectrum One in the range of 400-2500 cm^{-1}. Ultraviolet-visible (UV-Vis) absorption was measured on a PerkinElmer Lambda 900 UV-VIS-NIR spectrophotometer. Powder X-ray diffraction (PXRD) patterns were recorded on a Miniflex-600 diffractometer using Cu Kα radiation (λ = 0.154 nm). Xray photoelectron spectroscopy (XPS) measurements were performed on an ESCALAB 250 Xi X-ray photoelectron spectrometer (Thermo Fisher) using an Al Ka source (15 kV, 10 mA). N_2 adsorption-desorption isotherm and the Brunauer-Emmett-Teller (BET) surface area measurements were measured by using Micromeritics ASAP 2460 instrument. The nitrogen isotherms were measured at 77K, and the

samples were degassed in vacuum at 90 °C for 12 h. The CO_2 adsorption-desorption isotherms were measured up to 1 bar at 273 K and 298 K by using Micrometrics ASAP 2020 instrument. Scanning electron microscope (SEM) were recorded by a FEIT 20working at 10 KV. Transmission electron microscope (TEM) images were taken on a FEI TECNAI G2 F20 microscope equipped EDS detector at an accelerating voltage of 200 kV. The gas chromatography measurements were performed on the Agilent 7820A gas chromatograph (GC) equipped with FID and TCD. In situ Fourier transform infrared spectroscopy was obtained by Thermo Fisher. Gas Chromatography-Mass Spectrometer (GC-Mass) was obtained by Shimadzu QP2020.

The electrochemical measurements were performed in a H-type cell with two-compartments separated by a anion exchange membrance (Nafion-117) by chi700e at room temperature One compartment contained 70 mL electrolyte (0.5 M KHCO3 aqueous solution made from DI water) and Pt foil as counter electrodes, another with the same electrolyte, Ag/AgCl electrode in saturated KCl solution as reference electrodes and working electrode. Typically, 5 mg of the catalyst and 2 mg ketjenblack were dispersed in 1 mL of isopropanol and 50 μL of Nafion binder solution (5 wt%) under sonication for 1 h to form a homogeneous ink. Then 80 μL of the catalyst ink was loaded onto the carbon fiber paper electrode with 1×1 cm^2. During the electrochemical measurements, the electrolyte solution was purged with CO_2 for 30 min to achieve the CO_2-saturated solution (pH = 7.6). Linear sweep voltammetry (LSV) was performed with a scan rate of 10 mV s^{-1} from 0 V to -1.0 V vs. RHE in CO_2-saturated 0.5 M $KHCO_3$ electrolyte. All measured potentials were converted to reversible hydrogen electrode (RHE) scale using the following equation: E(vs. RHE)= E(vs. Ag/AgCl) + 0.059 pH + 0.197 V. CO_2 gas was delivered at an average rate of 30 ml/min (at room temperature and ambient pressure) and routed into the gas sampling loop (0.8 mL) of a gas chromatograph. The gas phase composition was analyzed by GC every 15 min. The separated gas products were analyzed by a thermal conductivity detector (for H_2) and a flame ionization detector (for CO, CH_4). The liquid products were analyzed afterwards by quantitative NMR (Bruker

AVANCE AV Ⅲ 400). Solvent presaturation technique was implemented to suppress the water peak.

Faradaic efficiency calculation for CO:

$$FE = \frac{J_{CO}}{J_{total}} = \frac{v_{co} \times N \times F}{J_{total}}$$

J_{CO} : partial current density for CO production;

J_{total}: total current density;

N: the number of electron transferred for product formation, in which it is 2 for CO;

v_{CO}: the production rate of CO (measured by GC);

F: Faradaic constant, 96485 C mol^{-1};

FE: Faradaic efficiency for CO production.

Evaluation of turnover frequency (TOF, h^{-1}) for CO:

$$TOF = \frac{I_{product}/NF}{m_{cat} \times \omega / M_{metal}} \times 3600$$

$I_{product}$: partial current for certain product, CO, the total current and Faraday efficiency of CO under the test potential were obtained through electrochemical test, then multiplication calculation to obtain $I_{product}$;

N: the number of electron transferred for product formation, in which it is 2 for CO;

F: Faradaic constant, 96485 C mol^{-1};

m_{cat}: catalyst mass in the electrode, g, the test dose we used was 400 μ g;

ω: metal loading in the catalyst, we get this data through ICP;

M_{metal}: atomic mass of metal.

Section S2. Chemical Synthesis

Synthesis of 5, 10, 15, 20-tetrakis (para-aminophenyl)-21H, 23H-porphyrin

(TAPP):

Following a modified procedure from reference[S1].

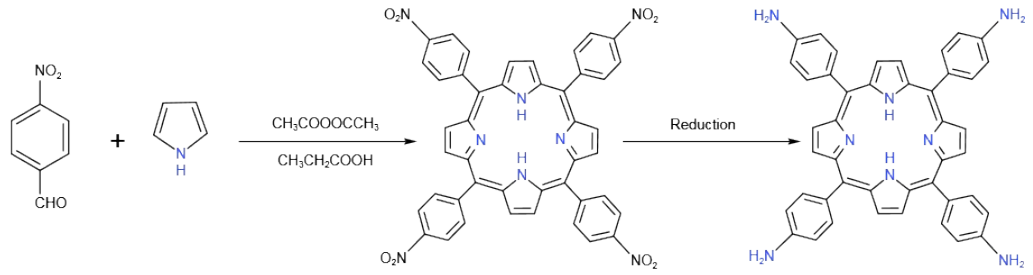

Scheme S1. Synthesis of TAPP

(1) Synthesis of 5,10,15,20-tetrakis (p-nitrophenyl)-21H, 23h-porphyrin (TNPP):

In a 500 mL flask, p-nitrobenzaldehyde (11 g, 0.07 mol), propionic acid (300 mL) and acetic anhydride (12 mL) were added and heat to 145 °C to reflux with stirring. Then the mixed solution with 5 mL of pyrrole and 10 mL of propionic acid was added and continue refluxing under stirring for 1h. After that cooled to room temperature and stand undisturbed for 24 h. Then the crude product was affording through vacuum filtered, then washed with 100 mL water for 6 times. Put the crude product in a 80°C vacuum oven for overnight to drying to obtain purple-black solid. After that, the solid was mixed with 80 mL of pyridine and refluxed for 1 h, then cooled to room temperature and stored at -4 °C overnight to get black precipitate. Then the solvent was removed through vacuum filtered and washed the filter cake with acetone for several times until the filtrate become colorless, yielding bright purple product TNPP.

(2) Synthesis of 5, 10, 15, 20-tetrakis (para-aminophenyl)-21H, 23H-porphyrin (TAPP):

The second step is the reduction of nitro to amino groups. 2.2 g of TNPP was dissolved in 100 mL of concentrated hydrochloric acid. 25 mL of concentrated hydrochloric acid solution containing 9.3 g of $SnCl_2 \cdot 2H_2O$ was added dropwise to the porphyrin solution within 10 min at room temperature under stirring, and then the temperature was raised to 70 °C for 1h. The dark green solid was separated by ice bath cooling, the hydrochloride was dispersed in 200 mL of deionized water, neutralized with concentrated ammonia to pH = 9, and the solid was collected by centrifugation and dried under vacuum at 70 °C. The product was extracted with 300

mL chloroform by using a Soxhlet extractor, and solvent was concentrated to 20 mL by rotary evaporation, it was recrystallized by adding 100 mL of diethyl ether to obtain of bright purple TAPP crystal. ^{1}H NMR (DMSO, 400 MHz): δ ppm 8.88 (s, 8H, pyrrole-C-H), 7.85 (d, J =8.1 Hz, 8H, Ar-H), 7.00 (d, J = 8.1 Hz, 8H, Ar-H), 5.58 (s, 8H, NH_2), -2.75 (s, 2H, pyrrole-N-H) (Figure S1), consistent with literature reports[S2].

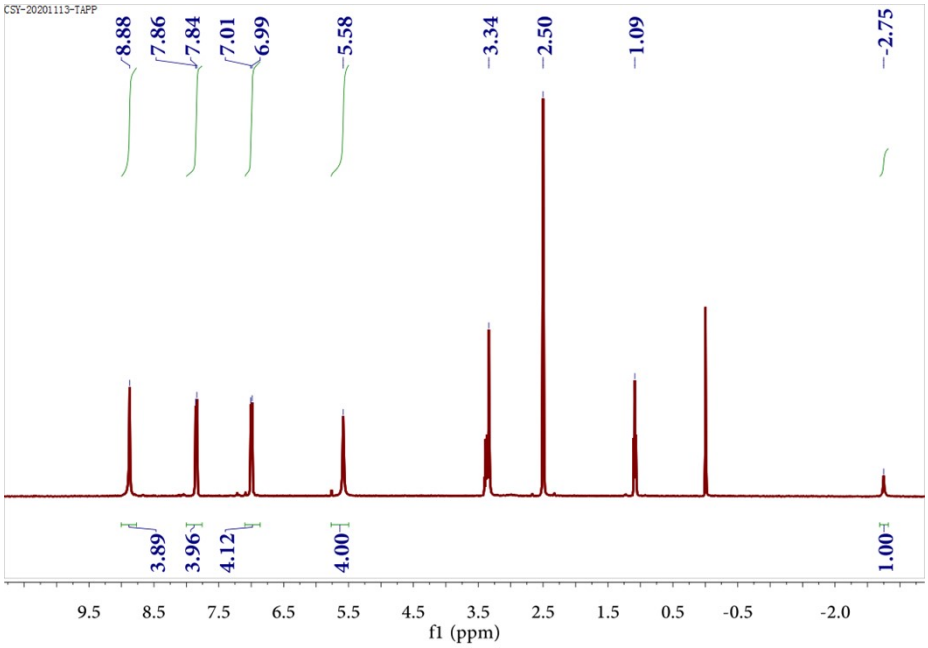

Figure S1. ^{1}H NMR spectrum of TAPP.

Synthesis of 5,10,15,20-tetrakis (4-aminophenyl) porphinato cobalt(II) (Co-TAPP):

Co-TAPP was synthesized according to reference and slightly modified. TAPP (200 mg, 0.30 mmol) and NaOAc (108 mg, 1.3 mmol) were added mixed solution with 63 mL of chlorobenzene and 45mL of DMF, then $Co(OAc)_2 \cdot 4H_2O$ (200 mg, 0.3 mmol) was added . After equipping with a Soxhelt apparatus with a paper thimble containing K_2CO_3 (1.1 g, 8.0 mmol), the reaction mixture was stirred under nitrogen at reflux for 24 h. Upon cooling, the Soxhlet apparatus was replaced with a distillation setup, and the solvent was removed under vacuum. The resulting dark solid was suspended in $CHCl_3$ (100 mL) and transferred to a Buchner funnel with a glass frit, and the solvent was removed through vacuum filtration. The crude product was then washed thoroughly with water three times, saturate $NaHCO_3$ solution one times, and then water again three times. The resulting dark purple microcrystalline powder was dried

under high vacuum overnight. The Q-band between 500 ~ 700nm is reduced to two characteristic peaks, and the Soret band shows a certain degree of blue shift, which is the most obvious feature of forming UV-Vis spectrum of metallic porphyrins (Figure S2).

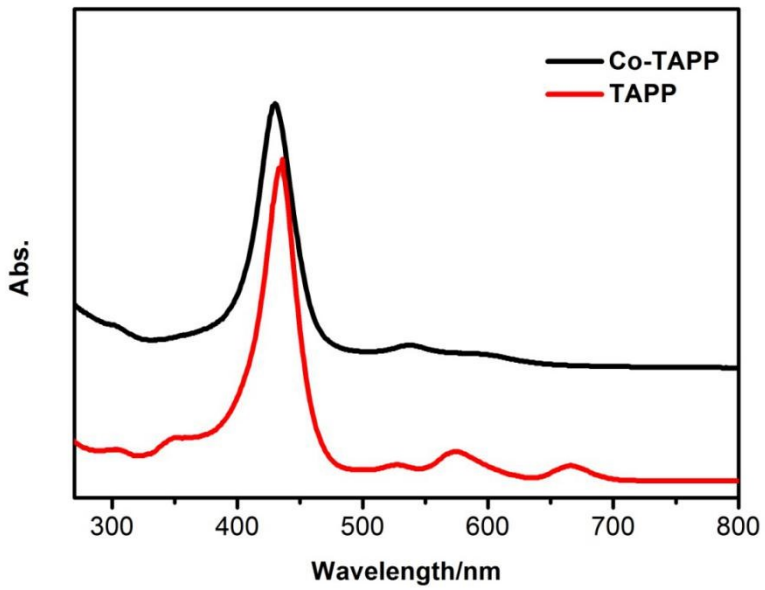

Figure S2. UV-Vis absorption spectra of TAPP (red line) and Co-TAPP (black line).

Synthesis of 3D COFs:

(1) Synthesis of 3D-Por(H)-COF:

A Pyrex tube 10 × 8 mm (o.d × i.d) was charged with TAPP (16.9 mg, 0.025 mmol) and TFPM (10.8 mg, 0.025 mmol), 1.8 mL *o*-dichlorobenzene, 0.2 mL *n*-butanol, and 0.2 mL of 6 M aqueous acetic acid. After sonication for 15 minutes the tube was flash frozen at 77 K (liquid N2 bath). After being degassed by freeze-pump-thaw technique for three times the system was evacuated to an internal pressure of 50 mTorr and flame sealed, the tube was placed in an oven at 120 °C for 5 d. The resulting precipitate was filtered off, exhaustively washed by Soxhlet extractions with tetrahydrofuran and dichloromethane for 2 d, dried at 70 °C under vacuum for overnight. The 3D-Por(H)-COF was isolated as a maroon powder.

(2) Synthesis of 3D-Por(Co/H)-COF:

A Pyrex tube 10 × 8 mm (o.d × i.d) was charged with TAPP (14.5 mg, 0.0214 mmol),

Co-TAPP (2.57 mg, 0.0036mmol) and TFPM (10.8 mg, 0.025 mmol), 1.8 mL *o*-dichlorobenzene, 0.2 mL *n*-butanol, and 0.2 mL of 6 M aqueous acetic acid. After sonication for 15 minutes the tube was flash frozen at 77 K (liquid N2 bath). After being degassed by freeze-pump-thaw technique for three times the system was evacuated to an internal pressure of 50 mTorr and flame sealed, the tube was placed in an oven at 120 °C for 5 d. The resulting precipitate was filtered off, exhaustively washed by Soxhlet extractions with tetrahydrofuran and dichloromethane for 2 d, dried at 70 °C under vacuum for overnight. The **3D-Por(Co/H)-COF** was isolated as a maroon powde.

(3) Synthesis of COF-366-Co:

COF-366-Co was synthesized according to reference[S3].

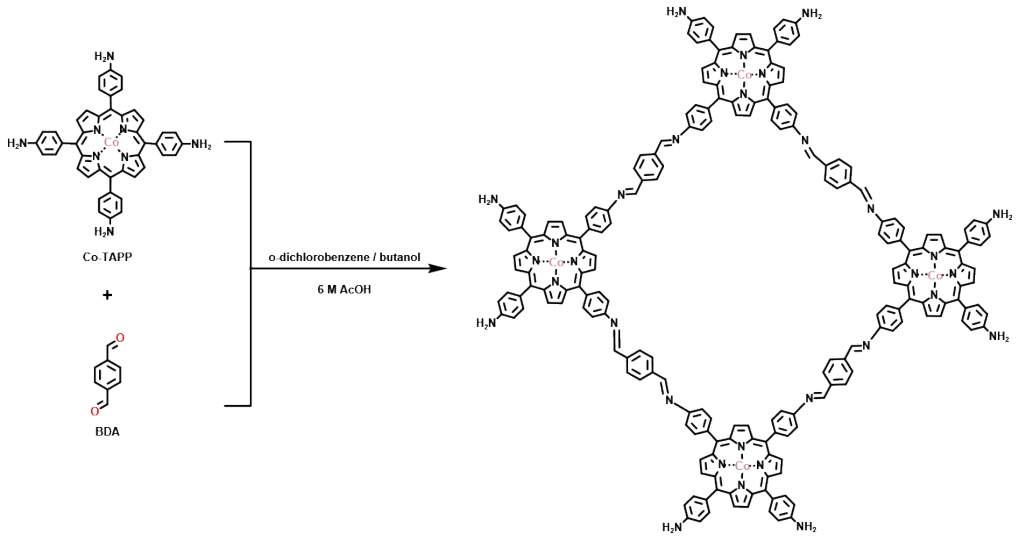

Scheme S2. Synthesis of COF-366-Co

A Pyrex tube measuring 10 × 8 mm (o.d × i.d) was charged with Co-TAPP (18 mg, 0.025 mmol), BDA (10 mg, 0.075 mmol), 1,2-dichlorobenzene (1 mL), butanol (1 mL), and 6 M aqueous acetic acid (0.25 mL). After sonication for 15 minutes the tube was flash frozen at 77 K (liquid N_2 bath). After one freeze-pump-thaw cycle the system was evacuated to an internal pressure of 50 mTorr and flame sealed. Upon sealing, the length of the tube was reduced to approximately 18~20 cm. The reaction was heated at 120 ºC for 48 h yielding a dark purple precipitate at the bottom of the tube, which was isolated by filtration. The wet sample was then transferred to a Soxhlet extractor and thoroughly washed with dioxane (24 h) and acetone (24 h),

dried at 70 °C under vacuum for overnight.

Section S3. Characterization of 3D-Por(H)-COF and 3D-Por(Co/H)-COF

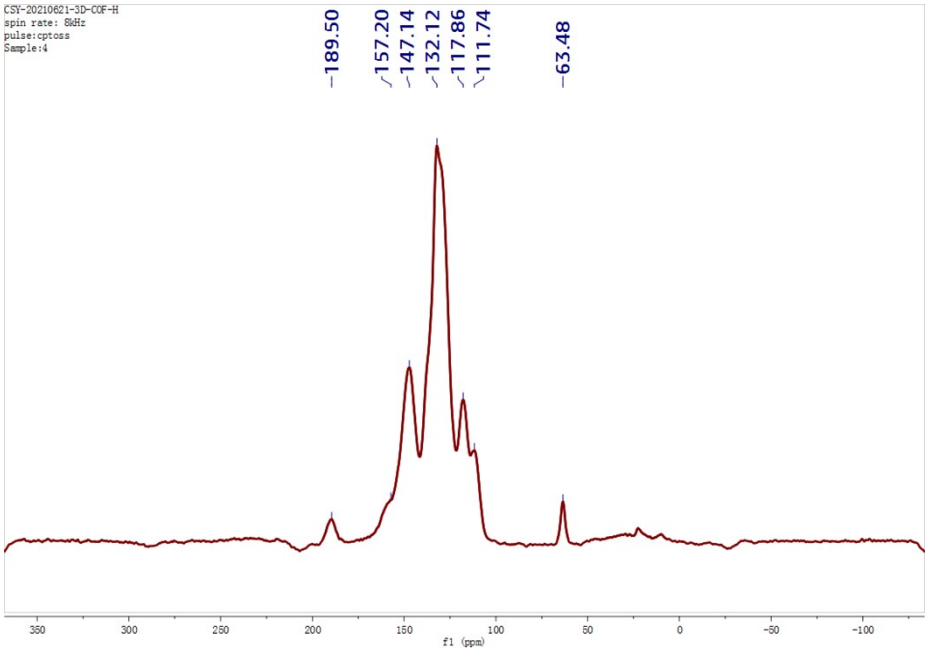

Figure S3. Solid-state 13C NMR spectra for 3D-Por(H)-COF.

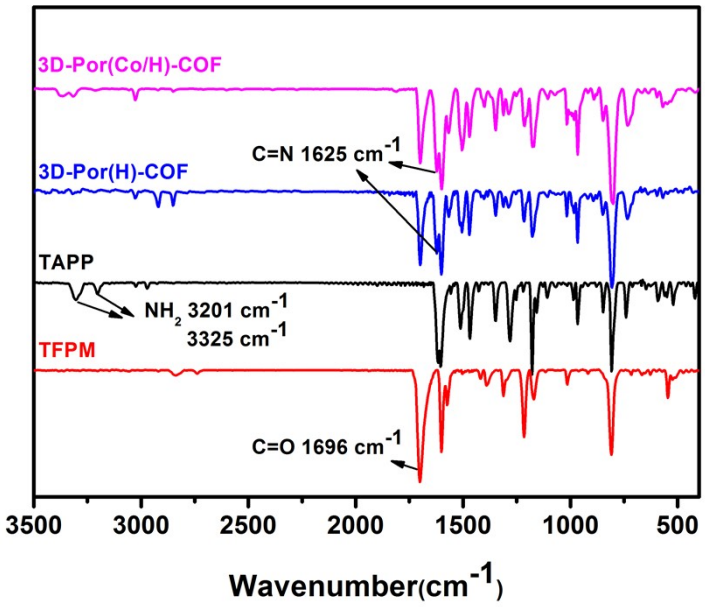

Figure S4. FT-IR spectra of TAPP (black curve), TFPM (red curve), 3D-Por(H)-COF (blue curve) and 3D-Por(Co/H)-COF (purple curve). The appearance of the band at about 1625 cm^{-1} confirmed the formation of imine linked C=N.

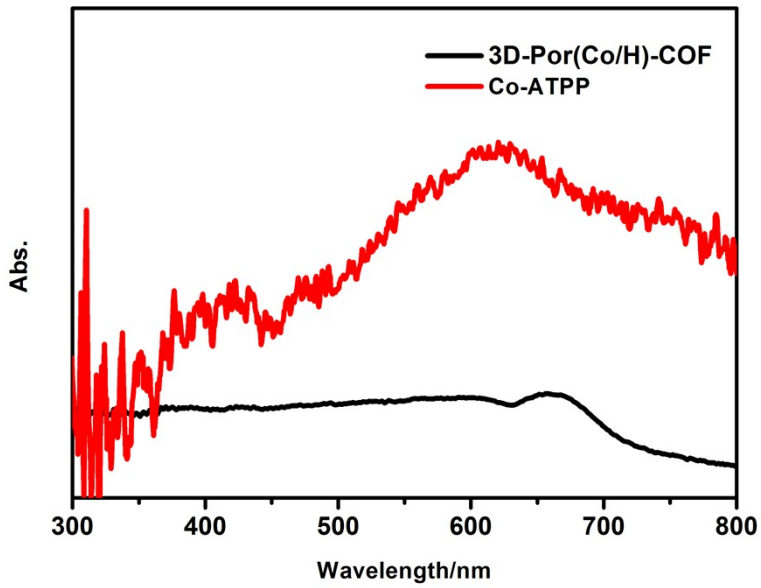

Figure S5. UV-Vis absorption spectra of 3D-Por(H)-COF (black line) and 3D-Por(Co/H)-COF (red line).

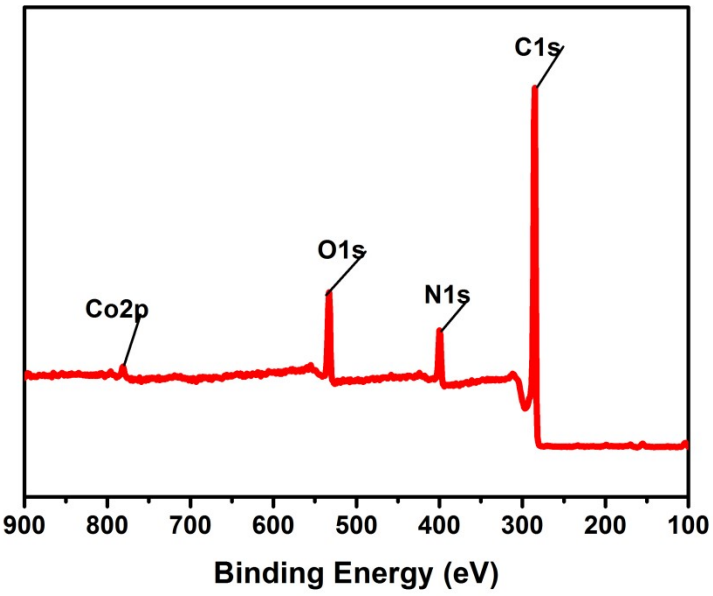

Figure S6. Survey XPS spectra of 3D-Por(Co/H)-COF.

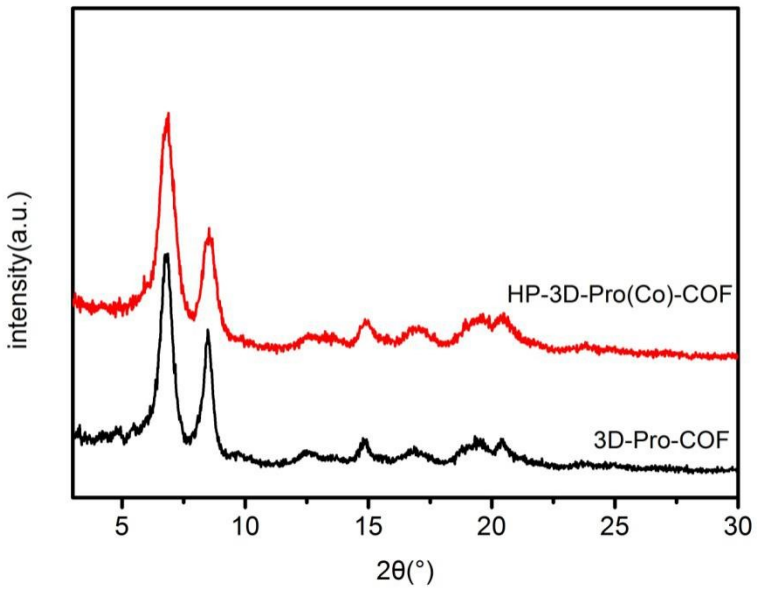

Figure S7. PXRD patterns of 3D-Por(H)-COF

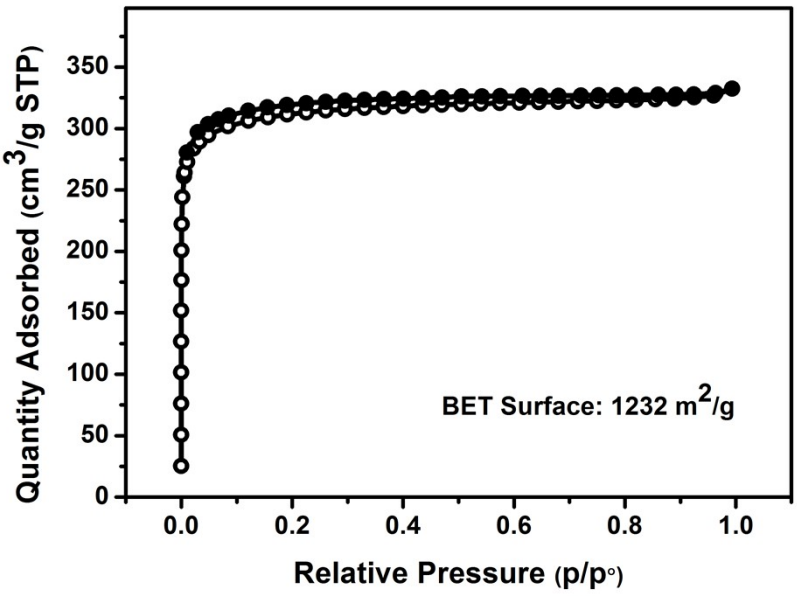

Figure S8. Nitrogen physisorption isotherms at 77 K for 3D-Por(H)-COF.

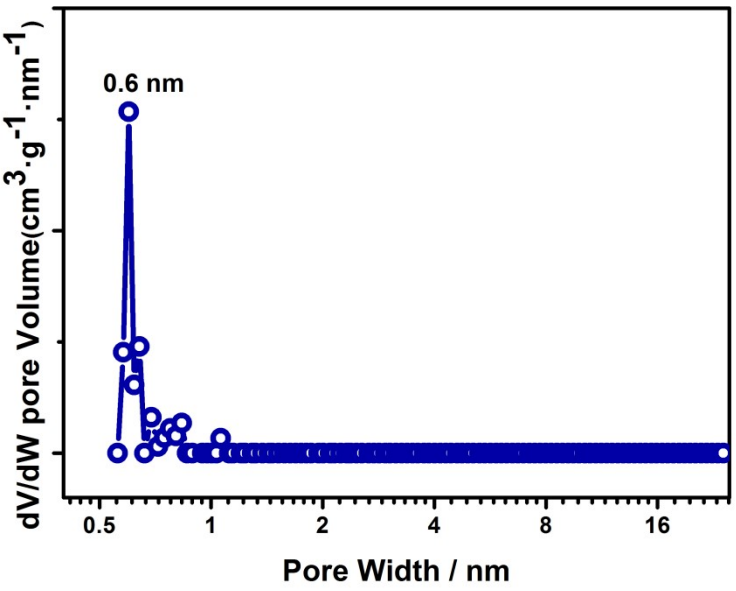

Figure S9. The pore-size distribution profile of 3D-Por(H)-COF.

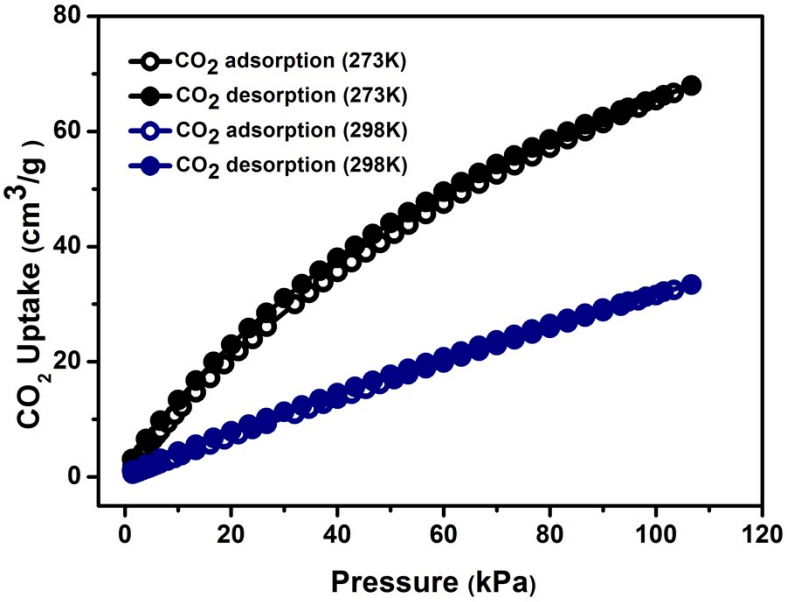

Figure S10. CO_2 physisorption isotherms of 3D-Por(H)-COF at 273 K (black line) and 298 K (blue line).

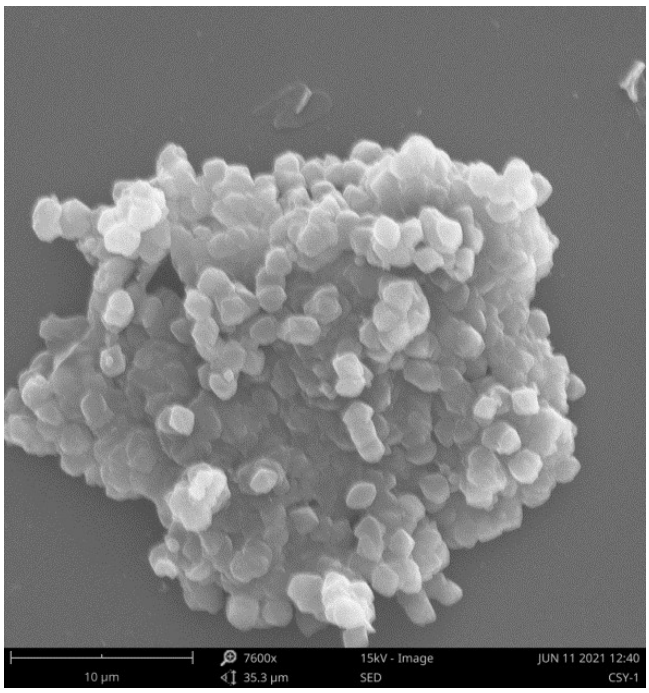

Figure S11. SEM images of 3D-Por(Co/H)-COF with scale bar 10 μm.

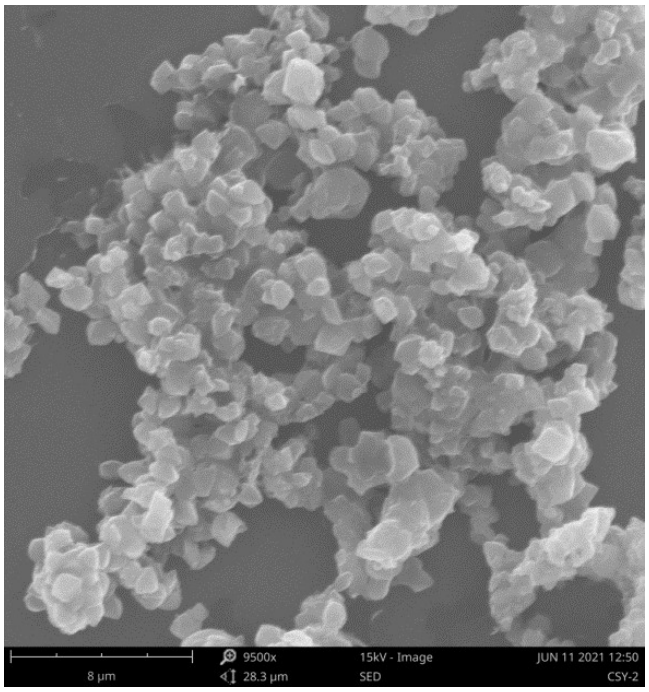

Figure S12. SEM images of 3D-Por(H)-COF with scale bar 8 μm.

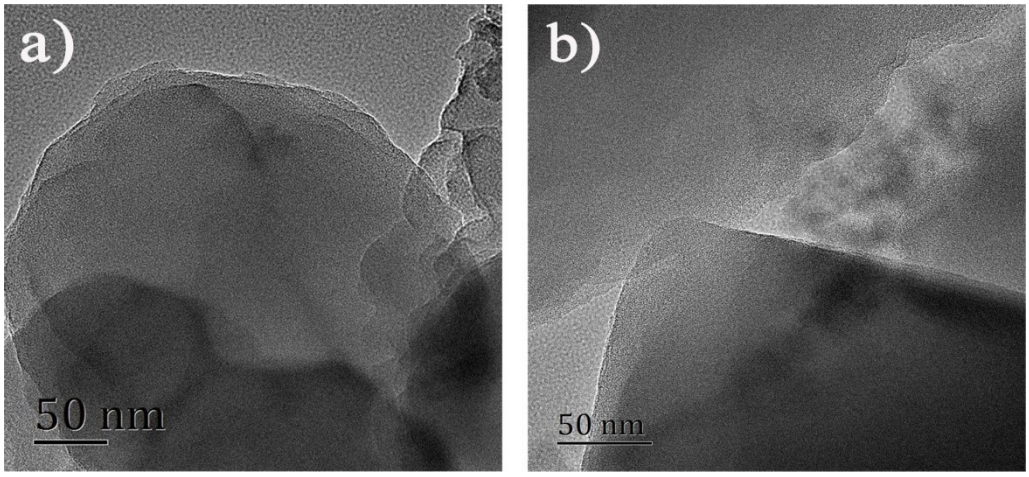

Figure S13. TEM of (a) 3D-Por(H)-COF and (b) 3D-Por(Co/H)-COF.

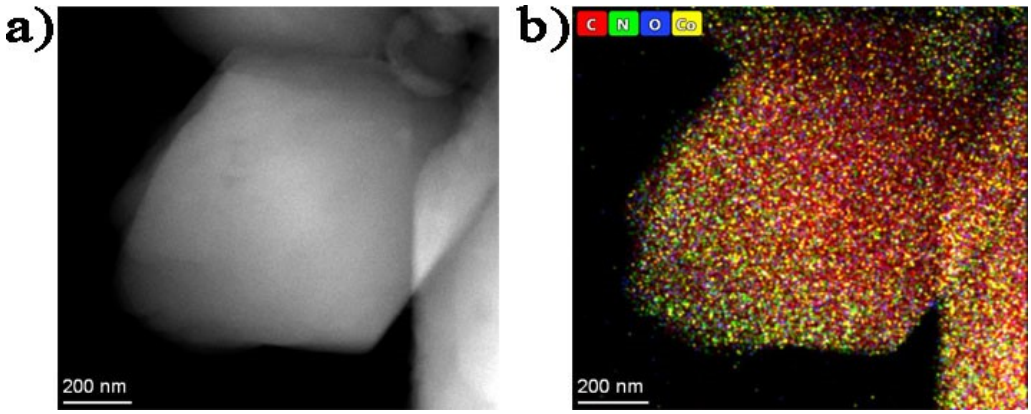

Figure S14. a) Corresponding high-angle annular darkfield scanning transmission electron microscopy (HAADF-STEM). b) EDS mapping of C, N, O and Co elements in selected area of 3D-Por(Co/H)-COF (dark field mode).

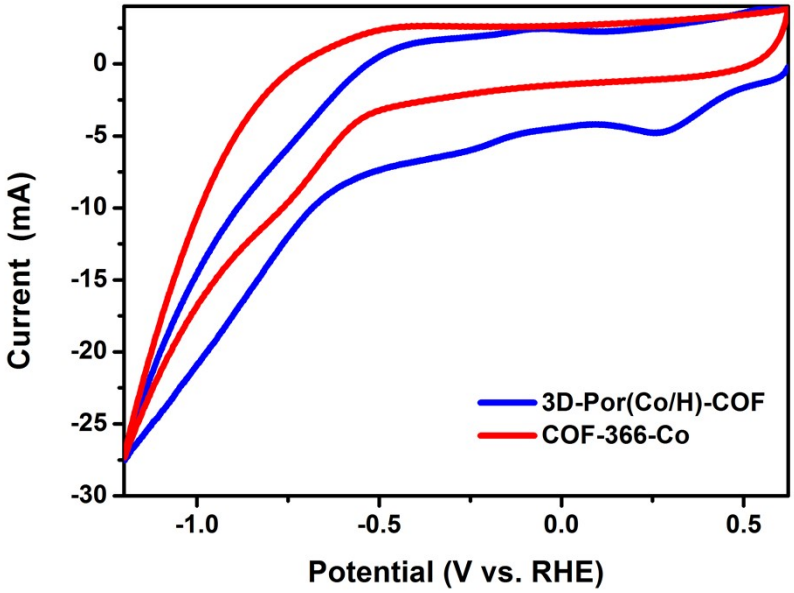

Figure S15. Cyclic voltammetry curves of the 3D-Por(Co/H)-COF (blue line) and COF-366-Co (red line).

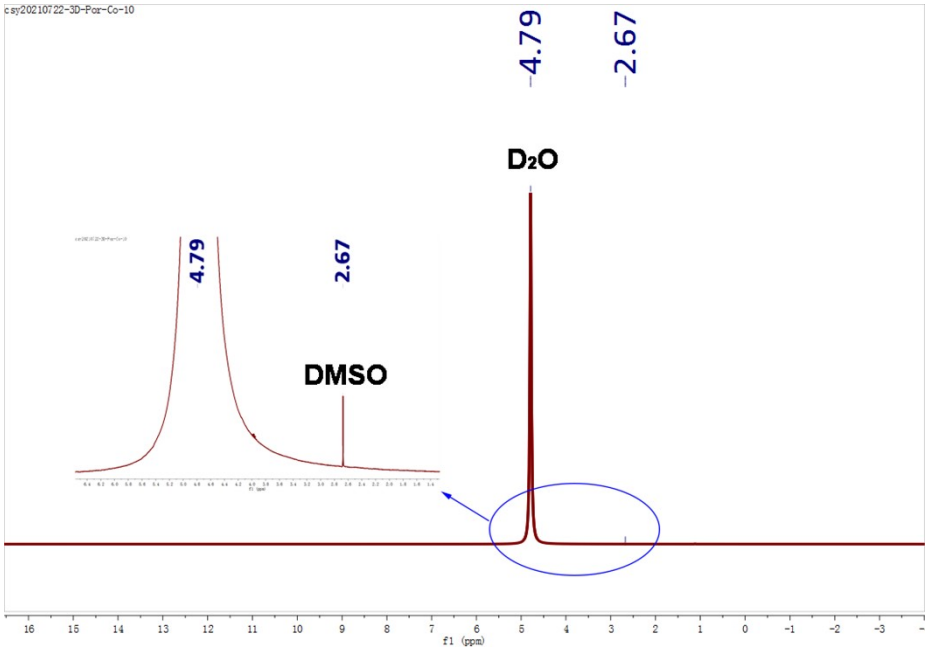

Figure S16. ^{1}HNMR spectrum of the electrolyte for 3D-Por(Co/H)-COF after CO_2RR testing.

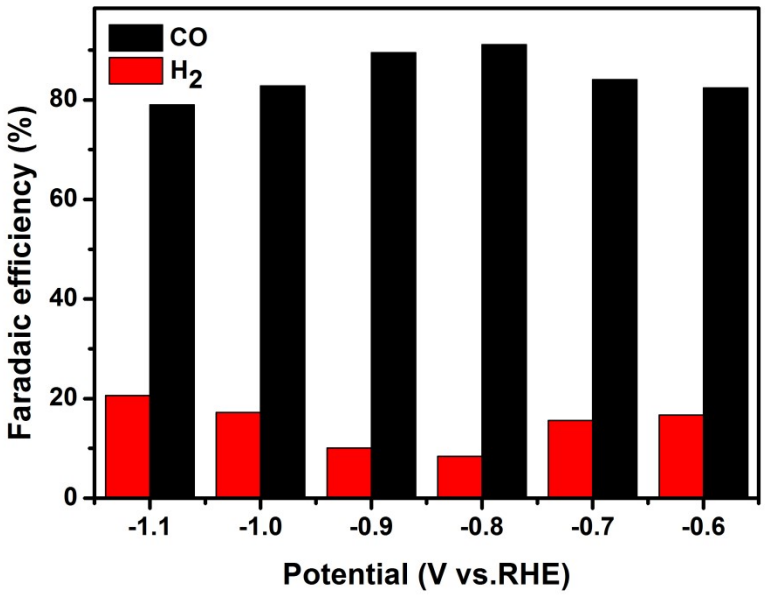

Figure S17. FEco from -0.6 V to -1.1 V vs. RHE of COF-366-Co.

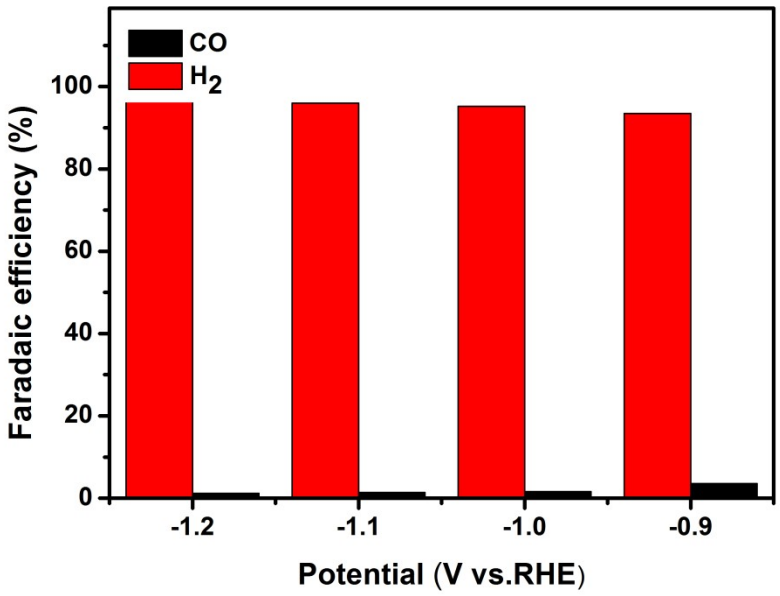

Figure S18. FEco from -0.6 V to -0.9 V vs. RHE of 3D-Por(H)-COF.

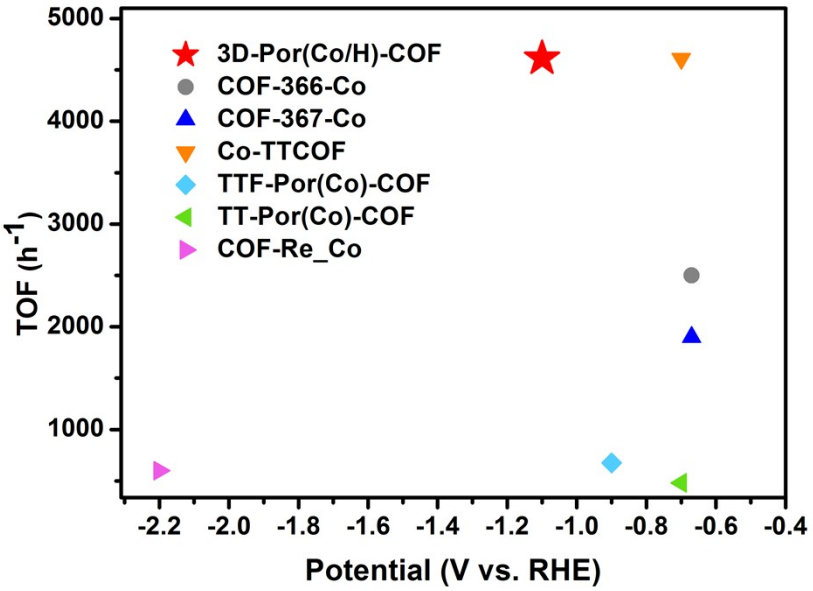

Figure S19. Comparison of TOF for CO_2 electroreduction.

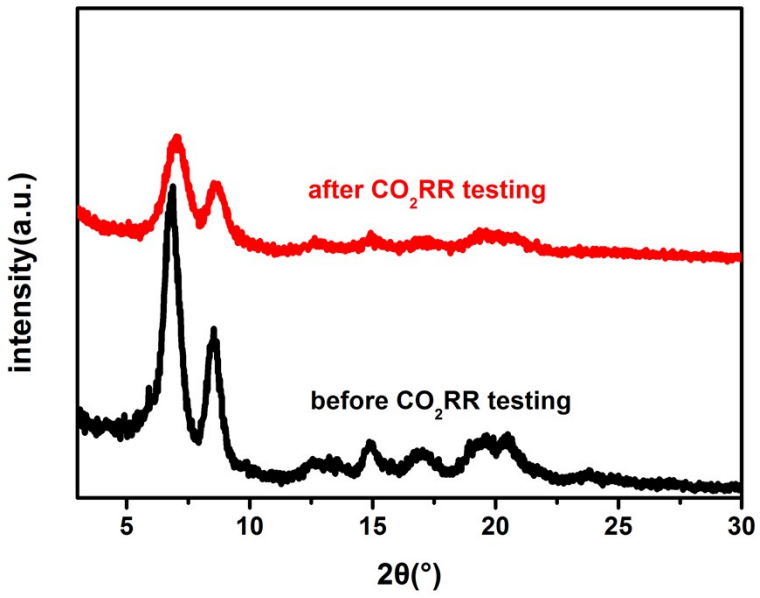

Figure S20. PXRD patterns of 3D-Por(Co/H)-COF before and after CO_2RR testing.

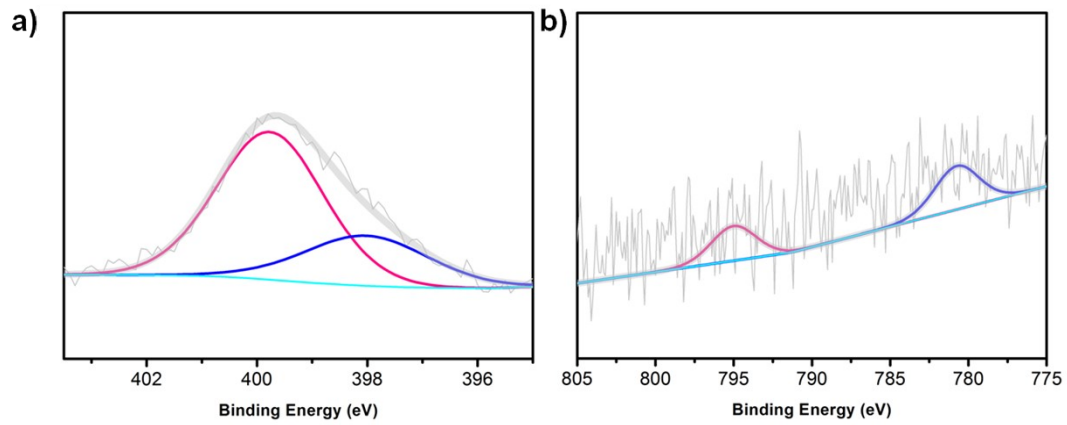

Figure S21. The XPS spectra of (a) N 1s; (b) Co 2p for 3D-Por(Co/H)-COF after CO_2RR testing.

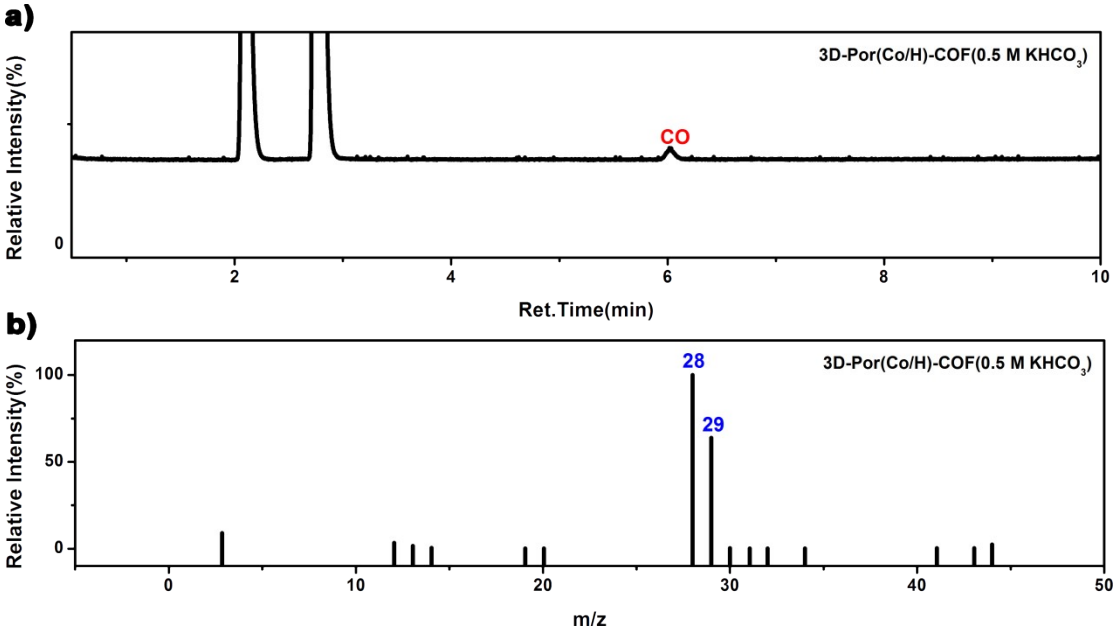

Figure S22. (a) The gas chromatography and (b) Mass spectrometry of 3D-Por(Co/H)-COF text in 0.5 M $KHCO_3$.

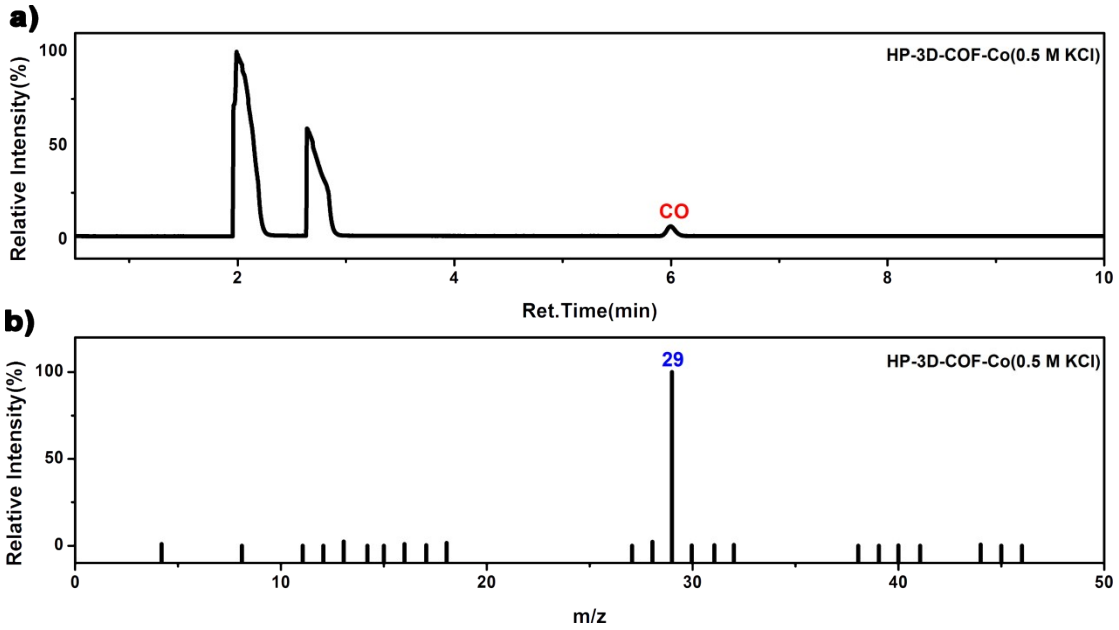

Figure S23. (a) The gas chromatography and (b) Mass spectrometry of 3D-Por(Co/H)-COF text in 0.5 M KCl.

Table S1. Fitting results based on EXAFS analysis of 3D-Por(Co/H)-COF

Sample	Path	CN	$\sigma^2(10^{-3}Å^2)$	ΔE_0(eV)	R factor
3D-Por(Co/H)-COF	Co-N	3.84±0.80	0.0095±0.0022	31.56±2.94	0.0195

CN: coordination number; σ^2:Debye-Waller factor (a measure of thermal and static disorder in absorber-scatterer distances); ΔE_0: the inner potential correction; R factor is used to value the goodness of the fitting.

Table S2. Comparison of CO Faradaic efficiency of various catalysts for CO_2 electroreduction.

Catalyst	**Electrolyte**	**Applied potential (V vs RHE)**	**Optimal FE_{CO} (%)**	**Highest J_{CO} [mA cm^{-2}]**	**Ref.**
3D-Por(Co/H)-COF	**0.5 M $KHCO_3$**	**-0.6**	**92.4**	**15.5 (-**	**This**

				1.1 V)	**work**
COF-366-Co	0.5 M $KHCO_3$	-0.6	82.4	13.2 (-1.1 V)	This work
COF-367-Co	0.5 M $KHCO_3$	-0.67	91	3 (-0.67 V)	[3]
COF-366-Co(10%)	0.5 M $KHCO_3$	-0.67	70	0.56 (-0.67 V)	[3]
COF-366-Co(1%)	0.5 M $KHCO_3$	-0.67	40	0.16 (-0.67 V)	[3]
Co-TTCOF	0.5 M $KHCO_3$	-0.7	91.3	~4.25 (-0.9 V)	[4]
Co-TTCOF NSs	0.5 M $KHCO_3$	-0.8	99.7	--	[4]
TTF-Por(Co)-COF	0.5 M $KHCO_3$	-0.7	95	~6.88 (-0.9 V)	[5]
TT-Por(Co)-COF	0.5 M $KHCO_3$	-0.6	91.4	7.28 (-0.7 V)	[6]
COF-Re_Co	pH 7.2 aqueous phosphate buffer solutions whit 0.5 M $KHCO_3$	-0.67	18	~0.18 (-0.68 V)	[7]
COF-366-F-Co	0.5 M $KHCO_3$	-0.67	87	65 mA mg^{-1} (-	[8]

				0.67 V)	
COF-300	0.5 M $KHCO_3$	-0.85	27	~0.12 (-0.85 V)	[9]
COF-300-AR	0.5 M $KHCO_3$	-0.85	80	~1.75 (-0.85 V)	[9]

Table S3. Comparison of the turnover frequencies (TOFs) of literature reported 2D-COFs electrocatalysts and 3D-Por(Co/H)-COF.

Catalyst	**Electrolyte**	**Product**	**Applied potential [V vs. RHE]**	**Highest TOF [h^{-1}]**	**Ref.**
3D-Por(Co/H)-COF	**0.5 M $KHCO_3$**	**CO**	**-1.1**	**4610**	This work
COF-366-Co	0.5 M $KHCO_3$	CO	-0.67	2500	[3]
COF-367-Co	0.5 M $KHCO_3$	CO	-0.67	1900	[3]
COF-366-Co(10%)	0.5 M $KHCO_3$	CO	-0.67	4400	[3]
COF-366-Co(1%)	0.5 M $KHCO_3$	CO	-0.67	9400	[3]
Co-TTCOF	0.5 M $KHCO_3$	CO	-0.7	4608	[4]
TTF-Por(Co)-COF	0.5 M $KHCO_3$	CO	-0.9	676	[5]
TT-Por(Co)-COF	0.5 M $KHCO_3$	CO	-0.7	481	[6]
COF-Re_Co	pH 7.2 aqueous phosphate buffer solutions whit	CO	--	--	[7]

	0.5 M $KHCO_3$				
COF-366-F-Co	0.5 M $KHCO_3$	CO	--	--	[8]
COF-366-$(OMe)_2$-Co	0.5 M $KHCO_3$	CO	--	--	[8]
COF-300	0.1 M $KHCO_3$	CO	--	--	[9]
COF-300-AR	0.1 M $KHCO_3$	CO	--	--	[9]
FeDhaTph-COF	MeCN solution with 0.5 M TEF	CO	-2.2 V vs. Ag/AgCl	> 600 h^{-1} mol^{-1}	[10]
NiPor-CTF	0.5 M $KHCO_3$	CO	--	--	[11]
TAPP-PPN	0.1 M $KHCO_3$	CO	--	--	[12]

*Note: in Table S3,S2 all potentials are versus to reversible hydrogen electrode (RHE) exceptspecified; both FE_{CO} and J_{CO} are the highest reported in corresponding literature; the COF-366-Co(10%) and COF-366-Co(1%) was prepared with Co-TAPP and 5,10,15,20-tetrakis(4-aminophenyl)porphinato copper(II) (Cu-TAPP), with Co/Cu (10/90) and (1/99), respectively; -- means not reported or not calculated due to limited data reported.

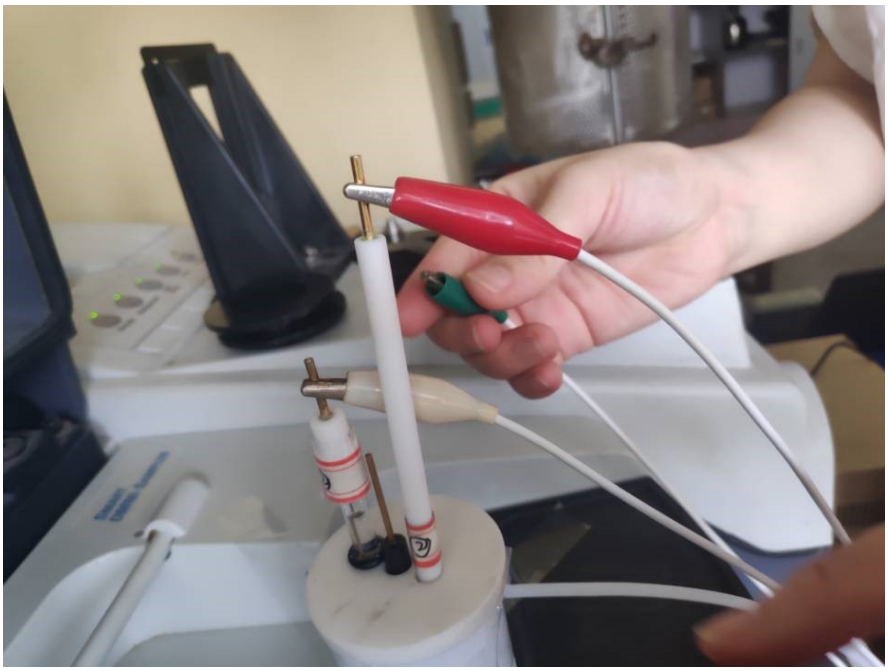

Figure S24. The home-made cell used for operando ATR-FTIR measurements. The ink was dropped on the glassy carbon electrode with silver chloride as the reference and platinum as the counterelectrode. Then, experiences were performed at -0.9 V in CO_2-saturated 0.5 M $KHCO_3$, gradually change the duration of the i-t test, and conduct an infrared test after each i-t test.

Section S4. Calculation method

The structures of intermediates were optimized by Density Functional Theory (DFT) through Gaussian09 program.[S13] The integral equation formalism of polarized continuum model (IEFPCM)[S14] as solvent model in conjunction with the B3LYP* functional[S15] were employed in all calculations. The Lanl2dz basis[S16,17] was chosen for Co atom, and 6-31G(d) basis[S18,19] was chosen for C, H, N atoms. The dispersion correction has been considered by using D3BJ.[S20,21]

As shown in Figure 5, the system was consisting of 1 cobalt atom, 44 carbon atoms, 8 nitrogen atoms and 32 hydrogen atoms. In CO_2RR and HER calculations, the system was optimized first, then the frequency was calculated. The structures were visualized by the VMD program. [S22]

Section S5. References

1 L. Zhao, T. Huang, Chemical Reagents, 2015, **37(9)** ,843 - 847.

2 Z. Cui， J. Zhou， T. Liu，Y. Wang， Y. Hu， Y. Wang， Z. Zou*, Chem-Asian J*., 2019, **14**, 2138-2148.

3 S. Lin, C. S. Diercks, Y. B. Zhang, N. Kornienko, E. M. Nichols, Y. Zhao, A. R. Paris, D. Kim, P. Yang, O. M. Yaghi, C. J. Chang, *Science*, 2015, **349**, 1208-1213.

4 H. J. Zhu, M. Lu, Y. R. Wang, S. J. Yao, M. Zhang, Y. H. Kan, J. Liu, Y. Chen, S. L. Li, Y. Q. Lan, *Nat. Commun.*, 2020, **11**, 497.

5 Q. Wu, R.-K. Xie, M.-J. Mao, G.-L. Chai, J.-D. Yi, S.-S. Zhao, Y.-B. Huang, R. Cao, *ACS Energy Lett.*, 2020, **5**, 1005-1012.

6 Q. Wu, M. J. Mao, Q. J. Wu, J. Liang, Y. B. Huang, R. Cao, *Small*, 2020, **17**, 2004933.

7 E. M. Johnson, R. Haiges, S. C. Marinescu, *ACS Appl. Mater. Interfacess*, 2018, **10**, 37919-37927.

8 C. S. Diercks, S. Lin, N. Kornienko, E. A. Kapustin, E. M. Nichols, C. Zhu, Y. Zhao, C. J. Chang, O. M. Yaghi, *J. Am. Chem. Soc.*, 2018, **140**, 1116-1122.

9 H. Liu, J. Chu, Z. Yin, X. Cai, L. Zhuang, H. Deng, *Chem*., 2018, **4**, 1696-1709.

10 P. L. Cheung, S. K. Lee, C. P. Kubiak, *Chem. Mater.*, 2019, **31**, 1908-1919.

11 C Lu，J Yang，S Wei，S Bi，Xia, Ying，Chen, Mingxi，Hou, Yang，Qiu, Ming，Yuan, Chris，Su, Yuezeng, *Adv. Funct. Mater.*, 2019, **29**, 1806884.

12 X. Cai, H. Liu, X. Wei, Z. Yin, J. Chu, M. Tang, L. Zhuang, H. Deng, *ACS Sustainable Chem. Eng.*, 2018, **6**, 17277-17283.

13 M. J. Frisch, G. W. Trucks, H. B. Schlegel, G. E. Scuseria, M. A. Robb, J. R. Cheeseman, G. Scalmani, V. Barone, G. A. Petersson, H. Nakatsuji, X. Li, M. Caricato, A. V. Marenich, J. Bloino, B. G. Janesko, R. Gomperts, B. Mennucci, H. P. Hratchian, J. V. Ortiz, A. F. Izmaylov, J. L. Sonnenberg, D. Williams-Young, F. Ding, F. Lipparini, F. Egidi, J. Goings, B. Peng, A. Petrone, T. Henderson, D. Ranasinghe, V. G. Zakrzewski, J. Gao, N. Rega, G. Zheng, W. Liang, M. Hada, M. Ehara, K. Toyota, R. Fukuda, J. Hasegawa, M. Ishida, T. Nakajima, Y. Honda, O. Kitao, H. Nakai, T. Vreven, K. Throssell, J. A. Montgomery, Jr., J. E. Peralta, F. Ogliaro, M. J. Bearpark, J. J. Heyd, E. N. Brothers, K. N. Kudin, V. N. Staroverov, T. A. Keith, R. Kobayashi, J. Normand, K. Raghavachari, A. P. Rendell, J. C. Burant, S. S. Iyengar, J. Tomasi, M. Cossi, J. M. Millam, M. Klene, C. Adamo, R. Cammi, J. W. Ochterski, R. L. Martin, K. Morokuma, O. Farkas, J. B. Foresman, and D. J. Fox, Gaussian, Inc., Wallingford CT, 2009.

14 J. Tomasi, B. Mennucci, R. Cammi, *Chem. Rev.*, 2005, **105**, 2999-3094.

15 A. D. Becke, *J. Chem. Phys.*, 1993, **98**, 5648-5652.

16 P. J. Hay and W. R. Wadt, *J. Chem. Phys.*, 1985, **2**, 299-310.

17 W. R. Wadt and P. J. Hay, *J. Chem. Phys.*, 1985, **2**, 284-98.

18 A. D. McLean, G. S. Chandler, *J. Chem. Phys.*, 1980, **72**, 5639-5648.

19 R. Krishnan, J. S. Binkley, R. Seeger, *J. A. Pople, J. Chem. Phys.*, 1980, **72**, 650- 654.

20 S. Grimme, *J. Comput. Chem.*, 2006, **27**, 1787-1799.

21 T. Schwabe, S. Grimme, *Phys. Chem. Chem. Phys.*, 2007, **9**, 3397-3406.

22 Humphrey, W., Dalke, A. and Schulten, K., *J. Molec. Graphics*, 1996, **14**, 33-38.